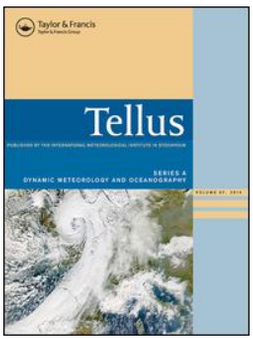

Tellus A: Dynamic Meteorology and Oceanography

ISSN: (Print) 1600-0870 (Online) Journal homepage: https://www.tandfonline.com/loi/zela20

On discretization error and its control in variational data assimilation

David Furbish, M. Y. Hussaini, F.-X. Le Dimet, Pierre Ngnepieba & Yonghui Wu

To cite this article: David Furbish, M. Y. Hussaini, F.-X. Le Dimet, Pierre Ngnepieba & Yonghui Wu (2008) On discretization error and its control in variational data assimilation, Tellus A: Dynamic Meteorology and Oceanography, 60:5, 979-991, DOI: 10.1111/j.1600-0870.2008.00358.x

To link to this article: https://doi.org/10.1111/j.1600-0870.2008.00358.x

Published online: 15 Dec 2016.

Tellus SERIES A DYNAMIC METEOROLOGY AND OCEANOGRAPHY
PUBLISHED BY THE INTERNATIONAL METEOROLOGICAL INSTITUTE IN STOCKHOLM

Tellus (2008), 60A, 979–991
Printed in Singapore. All rights reserved

TELLUS

On discretization error and its control in variational data assimilation

By DAVID FURBISH[1], M. Y. HUSSAINI[2]*, F.-X. LE DIMET[3], PIERRE NGNEPIEBA[4] and YONGHUI WU[2], [1]*Department of Earth and Environmental Sciences, Vanderbilt University, USA;* [2]*School of Computational Science, Florida State University, Tallahassee, FL 32306-4120, USA;* [3]*Laboratoire Jean-Kuntzmann, Université de Grenoble and INRIA, Grenoble, France* [4]*Department of Mathematics, Florida A&M, Tallahassee, FL 32307, USA*

(Manuscript received 7 February 2008; in final form 10 July 2008)

ABSTRACT

In four-dimensional variational data assimilation (4D-Var), the model equations are treated as strong constraints on an optimization problem. In reality, the model does not represent the system behaviour exactly and errors arise due to physical approximations, discretization, variability of physical parameters, and inaccuracy of initial and boundary conditions. Errors are also inherent in observation due to inaccuracies in the direct measurement and mapping of the state (model) space onto the observational space or vice versa. The purpose of this work is to define these errors, in particular the discretization and projection errors, and to formulate a canonical problem to study their impact on the quality of the data assimilation process and resulting predictions.

1. Introduction

Geophysical problems have two basic properties that should be kept in mind while seeking their numerical solution. First, they are irreducibly non-linear. Consequently, they do not possess global properties such as proper modes of linear models, nor do they have any asymptotic or periodic solutions. However, they do possess local existence and uniqueness properties, which hold in the neighbourhood of an initial state that is consistent with the given data/observation. Second, every geophysical state is unique. Therefore, a model cannot be validated by a single observation/data set. Validation requires an ensemble of independent observations (experiments).

1.1. Model and observation

The numerical forecast of geophysical flows is composed of three key elements—a mathematical model (and its discretized version), observation/data, and their statistics. These elements may be considered as heterogeneous representations of the same object/situation, and in the process known as data assimilation, they are combined together to obtain the initial condition/state, from which the numerical integration of the model equation proceeds for prediction purposes. Two critical questions arise that bear on the quality of prediction.

(i) What is the impact of discretizational, observational and model errors on the prediction?
(ii) Is it necessary to improve the model or the resolution of its discretization (number of grid points whereon the model is discretized) to obtain a better prediction?

Recently, there have been some attempts to answer the former question (Tribbia and Baumhefner, 1988; Griffith and Nichols, 2000; Nicolis, 2003). However, the latter question is seldom asked, because the answer is implicitly assumed to be in the affirmative. This work is an attempt to address specifically the discretizational and projection errors in a canonical context where the aforementioned errors can be defined precisely and their impact examined within the framework of 'exact' solutions of canonical equations.

1.2. Errors

Errors are obviously inherent in both the model and data. They affect the data assimilation process and, thereby, the accuracy of prediction. Model errors essentially stem from four distinct sources.

*Corresponding author.
e-mail: mhy@scs.fsu.edu
DOI: 10.1111/j.1600-0870.2008.00358.x

(i) Model errors due to the physical approximations underlying the primary model and/or auxiliary model that parametrizes subgrid scale phenomena.

(ii) Discretization errors due to the discretization of the model equations and incomplete iterative convergence involved in the numerical solution process.

(iii) Projection error due to the mapping of the state space on to the observational space.

(iv) Errors due to the indeterminacy of initial conditions; specifically, errors due to the initial guess (in other words, errors in the background term).

(v) Errors in observation/data resulting from the limitations of measurement tools and techniques or sampling errors.

Although the aforesaid errors are, in principle, independent, they are nevertheless intricately coupled as the mathematical model (barring analytical solutions) has to be discretized on a finite grid (or projected on to a finite dimensional space). The data assimilation process further entails interaction between these errors, which propagate through the trajectory and affect prediction. The problem of accounting for 'model error' (different from the definition given above) in variational data assimilation began to receive increasing attention in the last decade (Dalcher and Kalnay, 1987; Deber, 1989; Griffith and Nichols, 2000; Nicolis, 2003). Studies on predictability in meteorological models have shown that the impact of 'model error' on forecast is indeed significant. In their studies, Dalcher and Kalnay (1987) have extended Lorenz's parametrization by including the effect of error growth due to model deficiencies. Their results lead to the conclusion that the predictability limit of a forecast might be extended by two or three days if the 'model errors' are reduced or eliminated, if possible. There is, however, a lack of quantitative information on 'model error' in such forecast models.

The purpose of the ongoing research is to identify some of these errors and quantify their impact on the data assimilation process and, consequently, on prediction. The theoretical framework proposed here can deal with improving prediction by controlling these errors. In the interest of space and time, this work is confined to discretization and projection errors.

In the section that follows, we recall the general equations of four-dimensional variational data assimilation (4D-Var) in the continuous form. Next, we develop the procedure for error control in the data assimilation process. In Section 4, we formulate the canonical problem governed by Burgers equation with a force term, which makes it a relevant test case for geophysical application. In Section 5, we describe the discretization scheme and solution verification. Section 6 discusses the influence of model resolution and projection error on data assimilation. It also includes the influence of observation resolution on data assimilation. Section 7 illustrates the error control procedure in the case of the canonical Burgers problem. The final section summarizes the results and provides some conclusions.

2. Data assimilation: variational approach

2.1. Basic technique

For the sake of simplicity, we consider a problem where both the model and the observation are continuous with respect to space and time. The statistical structure of the fields will not be directly taken into account. An extension to a situation closer to operational reality is technically straightforward. The flow is described by a state variable $\mathbf{u} \in \mathcal{H}$, a Hilbert space, and it satisfies the semi-discrete model equation (after spatial discretization)

$$\begin{cases} \dfrac{\mathrm{d}\mathbf{u}}{\mathrm{d}t} = F(x, \mathbf{u}), \quad t \in [0, T], \\ \mathbf{u}(0) = U, \end{cases} \tag{1}$$

where x is the spatial variable, and t is the time. The cost function comprises two terms; the first term is the background term (also called the regularization term in optimal control terminology), which represents the difference between the initial condition and the background; the second term represents the discrepancy between the solution of the model $\mathbf{u}$ and the observation X_{obs}:

$$J(U) = \frac{\alpha}{2}\left\|U - U_0\right\|^2_{\mathcal{H}} + \frac{1}{2}\int_0^T \left\|H\mathbf{u} - X_{\text{obs}}\right\|^2_{\mathcal{H}_{\text{obs}}} \mathrm{d}t, \tag{2}$$

where U_0 is the background of the initial condition U, the observation $X_{\text{obs}} \in \mathcal{H}_{\text{obs}} = L_2(0, T; \mathcal{H})$, and the observational operator H maps $\mathcal{H}$ to $\mathcal{H}_{\text{obs}}$.

The observation is assimilated by the minimization of J with respect to U. The minimization can be realized by the quasi-Newton method. The gradient of the cost function needed in the minimization process is obtained by introducing the adjoint variable $P \in \mathcal{H}$ as the solution of the adjoint model defined by (Le Dimet and Talagrand, 1986)

$$\begin{cases} \dfrac{\mathrm{d}P}{\mathrm{d}t} + \left[\dfrac{\partial F}{\partial \mathbf{u}}\right]^T P = H^T\left(HX - X_{\text{obs}}\right), \\ P(T) = 0. \end{cases} \tag{3}$$

Backward integration of the adjoint model permits one to compute the gradient of the cost function J with respect to the input U:

$$\nabla J(U) = -P(0) + \alpha(U - U_0). \tag{4}$$

It is important to point out that eqs (1), (3) and (4) form the optimality system (OS), which contains all of the available information: the model, the observation and the statistics through the choice of the metric. It must be considered as a generalized model and sensitivity studies should be carried out on the OS rather than on the model itself, especially if one is looking for sensitivity with respect to observational error.

3. Error control

Our error control approach is similar to that of Derber (1989). The spatially discrete state variable satisfies

$$\begin{cases} \dfrac{\mathrm{d}\mathbf{u}}{\mathrm{d}t} = F(x, \mathbf{u}) + E(x, t), \\ \mathbf{u}(0) = U, \end{cases} \tag{5}$$

where $E(x, t)$ is the error term. For the sake of simplicity, we assume that the model is perfect. Then we seek the optimal U and E, which minimize

$$J(U, E) = \frac{\alpha}{2}\|U - U_0\|^2 + \frac{1}{2}\int_0^T \|H\mathbf{u} - X_{\text{obs}}\|^2 \mathrm{d}t + \frac{\beta}{2}\int_0^T (E, E)\mathrm{d}t.$$

In principle, the optimal E satisfies $\nabla_E J(U, E) = 0$. To this end, we introduce the adjoint model,

$$\begin{cases} \dfrac{\mathrm{d}P}{\mathrm{d}t} + \left[\dfrac{\partial F}{\partial \mathbf{u}}\right]^T P = H^T (H\mathbf{u} - X_{\text{obs}}), \\ P(T) = 0, \end{cases}$$

which yields after some basic manipulation,

$$\begin{cases} \nabla_U J(U, E) = \alpha(U - U_0) - P(0), \\ (\nabla_E J, \delta E) = \displaystyle\int_0^T \int_\Omega \left(-\left[\frac{\partial (F(x, \mathbf{u}(t)) + E)}{\partial E}\right]^T P(t) + \beta E(x, t), \delta E \right) \mathrm{d}x\mathrm{d}t. \end{cases} \tag{6}$$

We assume that the error E lies in some subspace $\mathcal{E}$ of $\mathcal{H}$. Let X_i, $1 \le i \le K < N$, be a base of $\mathcal{E}$ and $\phi_j(t)$, $1 \le j \le L$, be some base in time. Then the model, including the error term, takes the form

$$\begin{cases} \dfrac{\mathrm{d}\mathbf{u}}{\mathrm{d}t} = F(\mathbf{u}) + \displaystyle\sum_{i,j} \varepsilon_{ij}\phi_j(t)X_i \\ \mathbf{u}(0) = U, \end{cases} \tag{7}$$

where ε_{ij} are constants to be determined. The cost function can be reformulated as

$$J(U, \Gamma) = \frac{\alpha}{2}\|U - U_0\|^2_{\mathcal{H}} + \frac{1}{2}\int_0^T \|H\mathbf{u} - X_{\text{obs}}\|^2_{\mathcal{H}_{\text{obs}}} \mathrm{d}t + \frac{\beta}{2}\sum_{i,j} \varepsilon_{ij}^2. \tag{8}$$

The last term in the definition of the cost function, is a penalty or regularization term. The optimality condition is obtained by using the same adjoint model as written in eq. (3). The integration of the adjoint model gives the optimality condition:

$$\nabla_U J(U, \Gamma) = \alpha(U - U_0) - P(0) \tag{9}$$

and

$$\nabla_{\varepsilon_{ij}} J(U, \Gamma) = \beta\varepsilon_{ij} - \int_0^T \phi_j(t)(X_i, P)\mathrm{d}t. \tag{10}$$

3.1. Choice of the bases

Equation (5) is the finite-difference analogue of the model equation, where an approximate expression for the error is (Warming and Hyett, 1974)

$$E \approx \sum_p \varepsilon(p)\nabla^p \mathbf{u}. \tag{11}$$

Specifically, the error term results from the discretization of the convection terms (first-order derivatives). If the discretization scheme is formally of first order, the highest order of numerical dissipation error is proportional to $\nabla^2\mathbf{u}$ and the numerical dispersion error is proportional to $\nabla^3\mathbf{u}$. If one would like to control the numerical dissipation error to obtain optimal initial conditions (so that numerical diffusion does not overwhelm the molecular diffusion), one may choose the eigenfunctions of the Laplacian operator as the basis functions X_i. If there is no a priori knowledge of the error, the eigenvectors of the error covariance matrix may be chosen as the basis. In general a model has several sources of error, which can be combined as follows.

$$\begin{cases} \dfrac{\mathrm{d}\mathbf{u}}{\mathrm{d}t} = F(x, \mathbf{u}) + \displaystyle\sum_{i,j} \varepsilon_{ij}^1 \phi_j^1(t) X_i^1 + \sum_{i,j} \varepsilon_{ij}^2 \phi_j^2(t) X_i^2 + \cdots \\ \mathbf{u}(0) = U, \end{cases} \tag{12}$$

where the bases X_i^n, $i = 1, 2, \ldots$ are appropriately chosen for the pertinent source of error. A similar analysis can be carried out on the choice of the function ϕ_i, which should be chosen according to the characteristic time scales of the model. A wavelet discretization could be useful in this regard (Paun et al., 2003).

4. Formulation of canonical problem

The numerical solution of the model equations includes discretization error, which depends on the order of the numerical scheme. The discretization error is quantified by a scalar parameter h, which is a measure of grid size, and an error bound of the form $R.h^p$, which can be obtained by a numerical analysis of the scheme.

The estimation of the prediction error, which is the deviation of a solution of the model from the observation, is carried out in the space of observation $\mathcal{H}_{\text{obs}}$, into which the solution space $\mathcal{H}$ is projected by the observational operator H, as defined above. Obviously, H depends on the space of the discrete solution. At first, it would appear that as the size of h decreases, the prediction should improve. That is, as the grid is refined, the discretization error decreases, thus improving the prediction. Should it improve? In order to shed some light on this question, we consider the Burgers equation, which ''... is the simplest mathematical

formulation of the competition between convection and diffusion" (Burgers, 1948; Platzman, 1964; Benton and Platzman, 1972). Specifically for the concrete data assimilation problem, we consider a generalized Burgers equation:

$$\begin{cases} \dfrac{\partial u}{\partial t} + \dfrac{1}{2}\dfrac{\partial (u^2 + au)}{\partial x} - \mu\left[\dfrac{\partial^2 u}{\partial x^2}\right] = f(x), \\ \qquad\qquad (x, t) \in (-1, 1) \times (0, \infty), \\ \text{Boundary Condition: } u(-1, t) = u(+1, t) = 0 \ \forall t \in (0, \infty), \\ \text{Initial Condition: } u(x, 0) = U, \\ J(U) = \inf_v J(v). \end{cases} \tag{13}$$

Here μ is the coefficient of viscosity (presently set to 0.001), and the coefficient $a(x)$ and the source term $f(x)$ are defined in the Appendix A, where the exact solution is also derived. [Burgers equation has been considered in the context of data assimilation by Leredde et al. (1998), Uboldi and Kamachi (2000), to mention a few.]

The cost function is defined by

$$J(U) = \frac{1}{2} W_1 \sum_{i=2}^{M-1} \left(U^i - U_0^i\right)^2 + \frac{1}{2} W_2 \sum_{s=1}^{2} \sum_{k=1}^{K_s} \left(\{H[u(t_s, x_k)]\} - X_s^k\right)^2. \tag{14}$$

Here s is the observation time level, and K_s is the observation number at time level s; U_0 is the background, and X_s^k is the kth component of the observation at time t_s; H is the observational operator, which maps the state space on to the observational space. In other words, H maps the state variable u defined on the grid points to the observational sites where the observation variable is defined. W_1 and W_2 are weights related to the error covariance matrix of the background field and the observation. The more accurate the background field (or observations), the larger W_1 (or W_2) is. In practical applications, the background is usually obtained through the integration of the model for a period up to the initialization time, and W_1 is, therefore, related to the inverse of the error covariance matrix of the model.

Here, we specify the background as the exact initial condition (A8) contaminated by noise characterized by a Gaussian distribution with mean zero and variance σ. Since the optimal solution that minimizes the objective function depends only on the ratio W_2/W_1, we set W_1 to unity without loss of generality. The determination of W_2 is more complex, as it is related not only to the observation and model errors but also to the projection error (due to the mapping of the model variables at grid points to the observational sites). For simplicity, we assume that the theoretical model is perfect. A set of observations X_{obs} are generated from the exact solution at $t = 0$ and 1 on a uniform grid with step size $h = 0.02$, and they are, therefore, error free. The observational operator H is simply an interpolation operator, and W_2 is influenced only by the discretization error and the projection error (due to interpolation). Since the observation is accurate, it is reasonable to assume that the projection error dominates when the grid resolves the solution with sufficient accuracy. We assume that $W_2 = 10$.

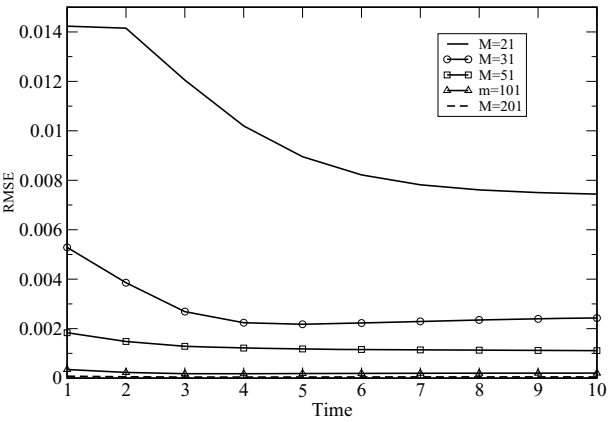

Fig. 1. Evolution of RMSE of the numerical solution for different resolutions. The initial conditions for all the solutions are exact.

5. Discretization scheme and solution verification

In the following, M denotes the total number of grid points (so that the spatial step is $\triangle x = 2/(M - 1)$) and u_j^n denotes the numerical solution of u at $(j\triangle x, n\triangle t)$. Central difference is used for spatial discretization, and the Euler scheme is employed for time discretization (Richtmyer and Morton, 1967). We choose $\triangle t = 0.005$ to satisfy the CFL condition, $\Delta t \leq \min\{\Delta \text{x/u}, \nu\, \Delta \text{x}^2/u\}$.

Verification of the forward solution. The exact initial condition is employed. Root mean square error (RMSE) of the numerical solution with respect to the exact solution at time $t = n\triangle t$ is defined as

$$\text{RMSE} = \sqrt{\frac{1}{M}\sum_{i=1}^{M}\left[u_{\text{ex}}(i \triangle x, n \triangle t) - u_i^n\right]^2}, \tag{15}$$

where $u_{\text{ex}}(x, t)$ is the exact solution of the forced Burgers eq. (A8). Figure 1 displays the evolution of the RMSE of the numerical solution with different model resolutions. It is noted that the RMSE decreases with increasing model resolution, as it should. Figure 2 plots four snapshots of both the exact and numerical solutions of various resolutions at times $t = 0$, 1, 2 and 5. Notice that as the number of grid points increases to 31, the numerical solution fairly captures the flow structures such as the crests and troughs, but not the amplitudes nor some of the finer structures. With a further increase in the number of grid points to 51 and beyond, the numerical solution agrees extremely well with the exact one.

In order to have an idea of the relative significance of the individual terms of the Burgers equation—non-linear convection

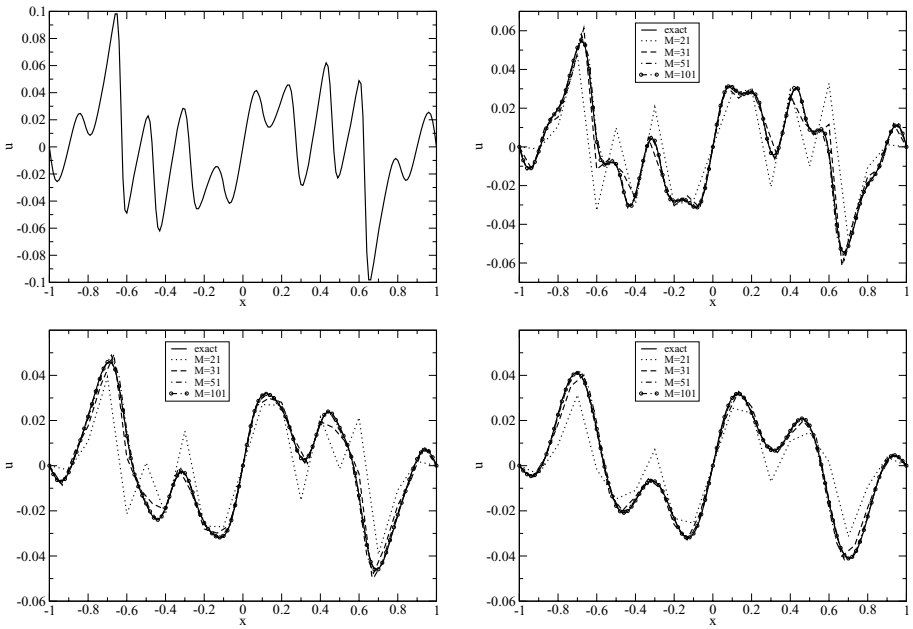

Fig. 2. (a) Exact solution of the forced Burgers equation at $t = 0$, and the exact and numerical solutions for different resolutions at (b) $t = 1$, (c) $t = 2$ and (d) $t = 5$. The initial conditions for all the solutions are exact.

$u\frac{\partial u}{\partial x}$, linear advection $\frac{\partial}{\partial x}(au)$, diffusion $\mu\frac{\partial^2 u}{\partial x^2}$, and the force term $f(x)$—as the solution evolves, we consider the sum of the absolute values of each of these terms over all the grid points relative to a similar sum of all of the terms:

$$S_1 = \sum_{i=1}^{M}\left|u_i^n\frac{\partial u_i^n}{\partial x}\right|,\quad S_2 = \sum_{i=1}^{M}\mu\left|\frac{\partial^2 u_i^n}{\partial x^2}\right|,$$
$$S_3 = \sum_{i=1}^{M}\left|\frac{\partial}{\partial x_i}\left[a(x_i)u_i^n\right]\right|,\quad \text{and}\quad S_4 = \sum_{i=1}^{M}|f(x_i)|. \tag{16}$$

Figure 3 illustrates the evolution of S_i/S, $i = 1, 2, 3, 4$ and $S = S_1 + S_2 + S_3 + S_4$. It is observed that in the present Burgers model, diffusion initially dominates. As time evolves, the solution becomes relatively smooth, and the linear advection term and the external force both become significant. Convection, although not very strong, plays an important role throughout the integration period.

Linear tangent model and adjoint code verification. Given the background U_0 of the initial condition, the minimization of the cost function, eq. (10), is carried out by the L-BFGS method (see Gilbert and Lemaréchal, 1989; Liu and Nocedal, 1989). The gradient of the cost function, required by the L-BFGS scheme, is obtained through the backward integration of the adjoint of the tangent linear model (TLM) of the original one. Two correctness checks on both the TLM code and its adjoint (ADJ) code are performed. First, we check if the equality (which is the definition of the adjoint operator):

$$(A\tilde{U}_0, A\tilde{U}_0) = \left(\tilde{U}_0, A^T A\tilde{U}_0\right), \tag{17}$$

is satisfied for any increment $\tilde{U}_0$ of the initial condition U. Here A represents the tangent linear approximation of the modified Burgers eq. (9) along with its solution $\mathbf{u}$, and A^T its adjoint. We choose $M = 101$ and $\tilde{U}_0$ to be one tenth of the exact initial condition (A8). The numerical result is that

$$\begin{aligned}(A\tilde{U}_0, A\tilde{U}_0) &= 1.338666125921017 \times 10^{-6}\\ \left(\tilde{U}_0, A^T A\tilde{U}_0\right) &= 1.338666125921016 \times 10^{-6},\end{aligned} \tag{18}$$

indicating 14-digit accuracy on a 32-bit machine.

The second check considers the formula,

$$D(\alpha) = \lim_{\alpha\longrightarrow 0}\frac{J(u+\alpha\tilde{U}_0) - J(u)}{\alpha\nabla J_u\cdot\tilde{U}_0} = 1, \quad \text{for } \forall\tilde{U}_0 \neq 0. \tag{19}$$

Observations are made at two instants—first at the initial time $t = 0$ and second at the end of the assimilation period $t = 1$. (Including observations in between 0 and 1 influences the results insignificantly.) There are 99 observational sites, which are uniformly distributed in the domain $(-1, 1)$. For the gradient check we take the background as 1.1 times the exact initial value plus a Gaussian noise with mean zero and variance 0.3. The convergence results of $D(\alpha)$ indicate seven-digit accuracy.

Finally, the L-BFGS method is employed for the minimization process. An example of the convergence history of both the cost function and its gradient norm for $M = 101$, and $\sigma = 0.003$ is listed in Table 1. This minimization method is very effective in that the cost function almost reaches its limit in the first five iterations, and the iterations thereafter only fine-tune it. In the following we choose the maximum number of iterations to be 50.

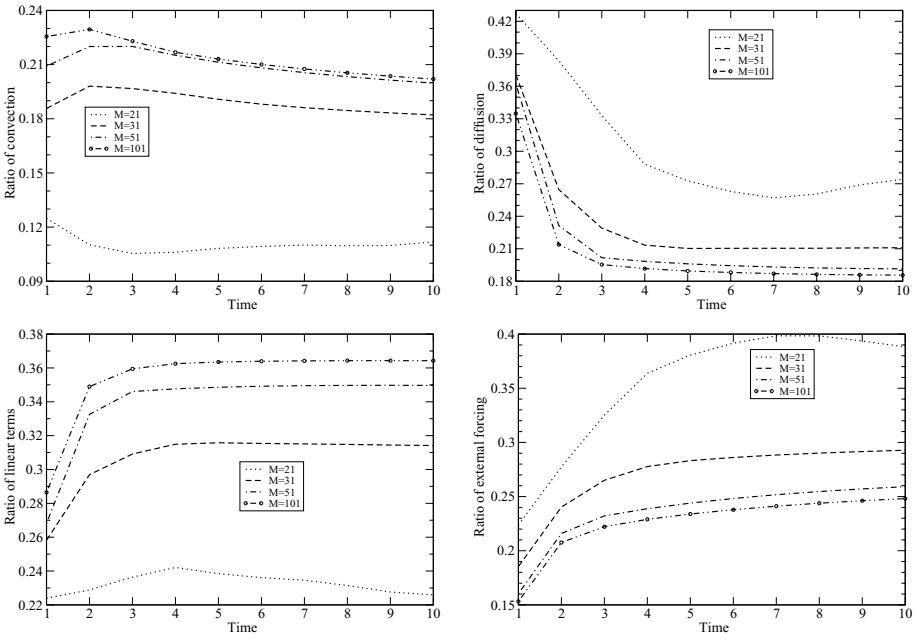

Fig. 3. Time evolution of the ratio of the sum of absolute value of terms (a) convection, (b) diffusion, (c) linear terms and (d) external forcing at each grid point to the summation of all the terms at each grid point.

Table 1. Convergence of both the cost function and the L^2-norm of its gradient in the case $M = 101$ and $\sigma = 0.025$

Iteration	J	$\|\nabla J\|$
0	0.35078592×10^{1}	0.17191152×10^{3}
1	0.35058595×10^{1}	0.17180853×10^{3}
2	$0.76635219 \times 10^{-1}$	0.30238631
3	$0.76601067 \times 10^{-1}$	0.30068101
4	$0.76298041 \times 10^{-1}$	0.28555660
5	$0.70462862 \times 10^{-1}$	$0.12666941 \times 10^{-2}$
6	$0.70451991 \times 10^{-1}$	$0.54982245 \times 10^{-3}$
7	$0.70446412 \times 10^{-1}$	$0.47975452 \times 10^{-4}$
8	$0.70446346 \times 10^{-1}$	$0.44660779 \times 10^{-4}$
9	$0.70445638 \times 10^{-1}$	$0.10635374 \times 10^{-4}$
10	$0.70445471 \times 10^{-1}$	$0.20295671 \times 10^{-5}$
11	$0.70445438 \times 10^{-1}$	$0.67729479 \times 10^{-7}$
12	$0.70445438 \times 10^{-1}$	$0.56747292 \times 10^{-8}$
13	$0.70445437 \times 10^{-1}$	$0.23630726 \times 10^{-10}$
14	$0.70445437 \times 10^{-1}$	$0.79286146 \times 10^{-12}$
15	$0.70445437 \times 10^{-1}$	$0.23419518 \times 10^{-13}$

6. Optimal model resolution

In this section, we address the question of whether or not there is an optimal resolution for the model given observations with a certain resolution. To that end, we assume that observation/data is available at 99 sites uniformly distributed in the interval $(-1, 1)$ at times $t = 0$ and 1. This observation/data is obtained from the exact solution and, hence, is error-free. We assume that the background U_0 is the exact initial condition (A8) contaminated by Gaussian noise with mean zero and variance σ. The only errors present are discretization and projection errors. The time window for data assimilation is set to 1, and the forecast time is $t = 5$. Equation set (9) is solved varying the resolution (number of discretization points). Optimal resolution is the optimal number of grid points, for which the discretization error represented by the RMSE (defined in (11)) of the numerical solution at $t = 0$ (or at $t = 1$) is minimal. Two different cases are considered: the first case is to determine the influence of the model resolution on the accuracy of data assimilation, and the second case is to determine the influence of projection/interpolation error on data assimilation.

6.1. *Influence of model resolution on data assimilation*

The observational operator H is assumed to be a linear interpolation operator, and the spatial resolution is varied from $M = 31$ to 201 grid points in the interval $(-1, 1)$.

Let us first examine the influence of the quality of the background, as determined by the error variance σ on the optimal solution (i.e. the solution with an optimal initial condition that is obtained from the data assimilation procedure). Figure 4 shows the RMSE of the optimal solution (with reference to the exact solution) versus the model resolution (the number of grid points) for perturbation variances $\sigma = 0.1$, 0.025, 0.0025 and 0.00025. A local minimum for RMSE at the initial time is observed (see Fig. 4). This local RMSE minimum is found to occur at $M = 101$ when the grid points of the discretized model coincide with the observational sites, resulting in zero projection/interpolation error. In other words, observational information is optimally

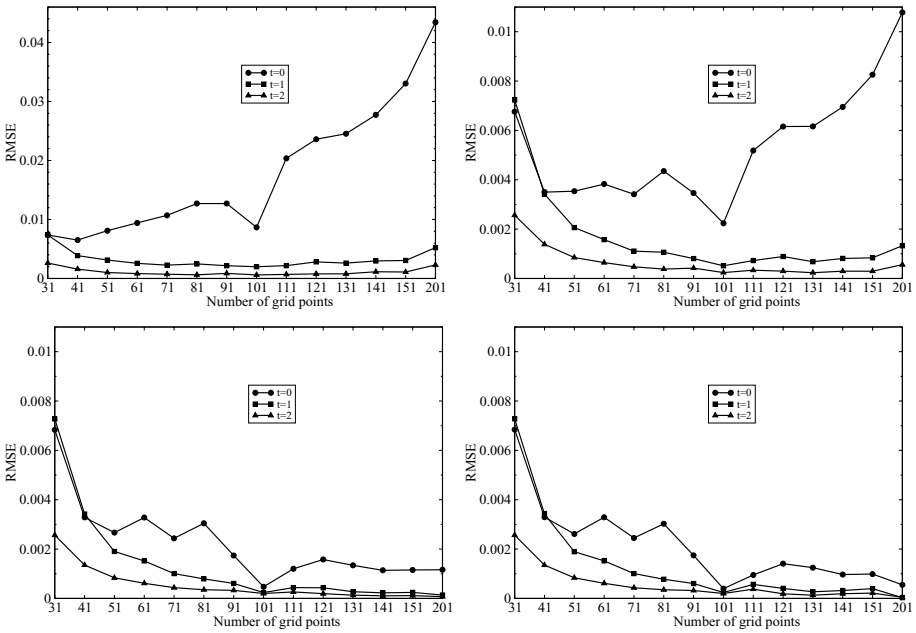

Fig. 4. RMSE of numerical solutions initialized with optimal initial condition at times $t = 0$, 1 and 2. The background field is the exact initial condition perturbed by Gaussian noise with mean zero and variance (a) $\sigma = 0.1$, (b) $\sigma = 0.025$, (c) $\sigma = 0.0025$ and (d) $\sigma = 0.00025$.

absorbed by the data assimilation process when the model resolution matches that of the observation. Moreover, it is observed in Fig. 4 that when the model resolution is coarse, the RMSE does not decrease with deceasing σ. This indicates that the optimal initial condition is not sensitive to the background when the observational sites are farther apart than the grid points whereon the model is discretized. As the model resolution increases beyond that of the observation, the RMSE quickly decreases with decreasing σ. This indicates that the optimal initial condition is sensitive to the background when the model resolution is finer than that of the observation. The reason is that when the model resolution is coarse, the minimization problem is overdetermined, and, therefore, the observations, if of good quality, determine the optimal initial condition uniquely. When the model resolution increases further, the minimization problem may become under-determined. Consequently there may exist many local minima of the cost function. Therefore, the optimal initial condition is sensitive to the background.

To illustrate the relationship between the optimal initial condition and the model resolution, we plot in Figs. 5–7 the exact solution, the optimal initial condition and the background for $\sigma = 0.025$ and 0.0025 at model resolutions of $M = 31$, 101 and 201, respectively. It is observed that for $M = 31$, that is, the model resolution is coarser than that of the observation, the optimal initial condition for $\sigma = 0.025$ is almost the same as that for $\sigma = 0.0025$, indicating that it is insensitive to the amplitude of the error in the background. It represents the structure of the exact initial condition well, but deviates from the exact one in amplitude. For $M = 101$, that is, the model resolution matches that of the observations, the optimal initial condition, independent of the background, corresponds well with the observations. For $M = 201$, the model resolution is finer than that of the observation, and the optimal initial condition for $\sigma = 0.025$ is quite different from that for $\sigma = 0.0025$, implying its insensitivity to the background. In the case $\sigma = 0.025$, the optimal initial condition agrees well with the exact solution at the grid points where there is observational data, while it depends on the background when there are no observations.

6.2. *Influence of observation resolution on data assimilation*

To investigate the influence of observation resolution, we carry out the data assimilation experiments (9) with fixed model resolution of 51 grid points and 101 grid points, and increase the resolution of observation from 49 through 99 to 199 grid points. The results on the RMSE of the numerical solutions on 51- and 101-point grids at times $t = 0$ and $t = 1$ are reported in Tables 2 and 3, respectively. The background field is the exact initial condition perturbed by Gaussian noise with mean zero and variance $\sigma = 0.025$ (the second and the third row) and $\sigma = 0.0025$ (the fourth and the fifth row). Table 2 shows that with the model resolution fixed at 51 grid points, increasing the resolution of observation does not translate into improved assimilation. However, with the model resolution fixed at 101 (see Table 3), increasing the observation resolution results in improved assimilation. It implies (see Fig. 4) that if the solution is sufficiently resolved (the 101 grid point case), the high density observations improves assimilation and affects it adversely otherwise.

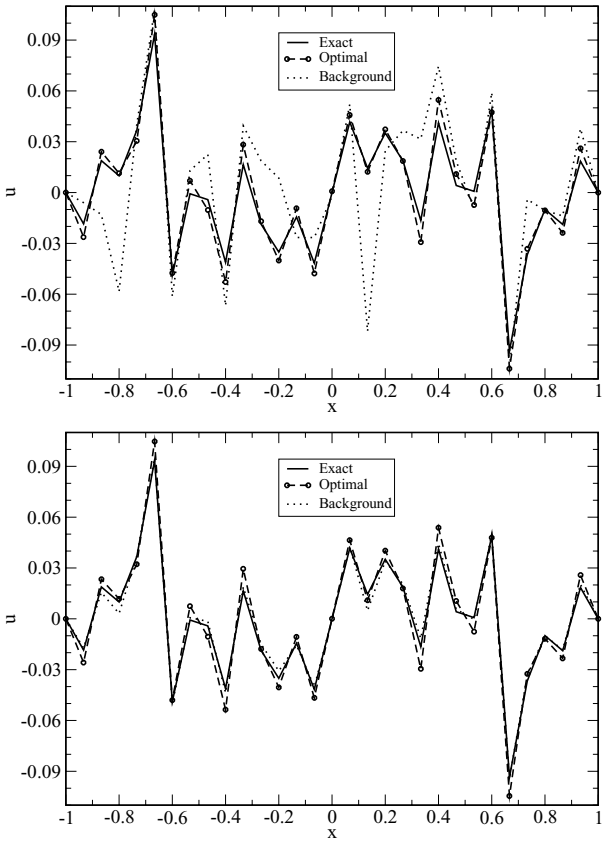

Fig. 5. Exact (black), optimized (dot–dashed), and the background (dash) of the initial fields for model resolution $M = 31$.

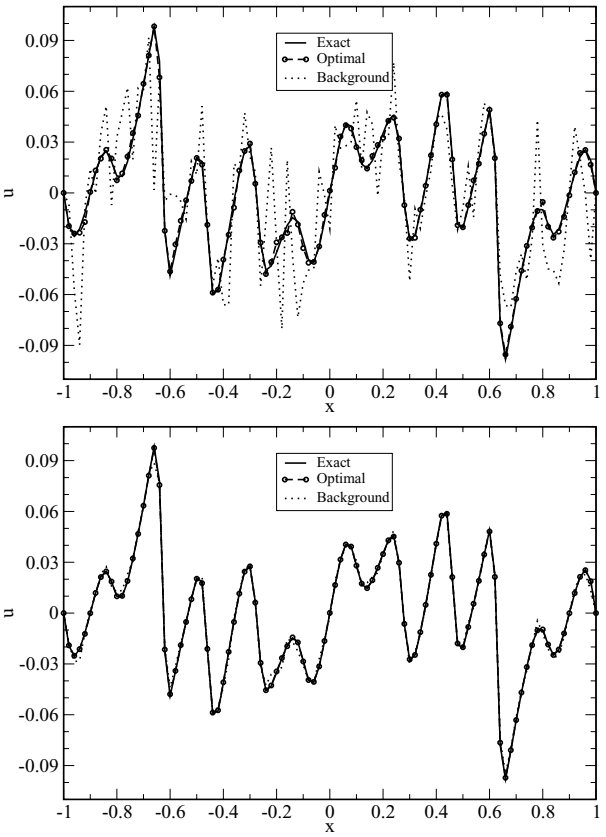

Fig. 6. Same as Fig. 5 except for the number of grid points $M = 101$.

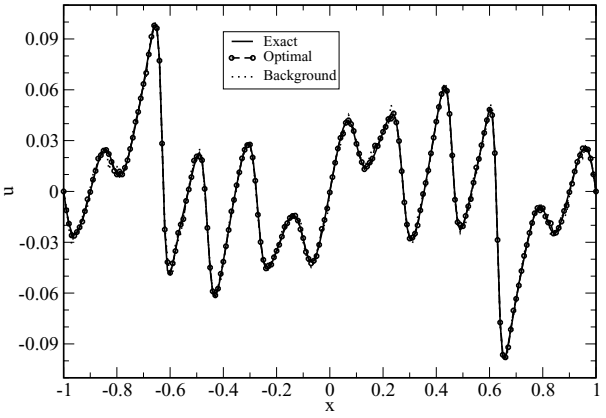

Fig. 7. Same as Fig. 5 except for the number of grid points $M = 201$ and $\sigma = 0.0025$.

6.3. *Influence of projection/interpolation error on data assimilation*

In the previous section, it was noted that the optimal initial condition is influenced by the projection error through the linear interpolation used to map the state space on to the observational space. Linear interpolation may entail significant errors when there are large gradient variations. Lagrange non-linear interpolation may then be appropriate to reduce the projection/interpolation error. In this case, we choose the observational operator H as a fourth-order non-linear Lagrange interpolation operator. Figure 8 shows the RMSE of the interpolation of exact solutions with different resolution to the observations at times $t = 0$ and 1. It is observed that the RMSE associated with Lagrange interpolation is less than the RMSE by linear interpolation. Moreover, for $M = 101$ and 201, there are no projection/interpolation errors since the model grid points coincide with the observational sites. The closer the resolution is to the observation, the less is the projection/interpolation error.

Figure 9 plots the RMSE of the optimal initial condition (with reference to the exact one) for different interpolation operators and variances $\sigma = 0.025$ and 0.0025. The RMSE is reduced when Lagrange interpolation is used, especially when the number of grid points is less than, but close to, $M = 101$. Moreover, when the model resolution approaches that of the observation, the RMSE reaches a local minimum. This substantiates the existence of the optimal resolution of the model no matter what kind of interpolation is used.

The jump in the RMSE at $M = 61$ and 81 in Fig. 9 needs further explanation (see also Fig. 4). It is due to the fact that the

Table 2. RMSE of the numerical solution on 51-point grid

Obs number	49	99	199
$t = 0$	0.1597×10^{-2}	0.2952×10^{-2}	0.3144×10^{-2}
$t = 1$	0.1282×10^{-2}	0.1286×10^{-2}	0.1323×10^{-2}
$t = 0$	0.1277×10^{-2}	0.2835×10^{-2}	0.3110×10^{-2}
$t = 1$	0.1244×10^{-2}	0.1263×10^{-2}	0.1314×10^{-2}

Table 3. RMSE of the numerical solution on 101-point grid

Obs number	49	99	199
$t = 0$	0.4467×10^{-2}	0.2817×10^{-2}	0.1718×10^{-2}
$t = 1$	0.1204×10^{-2}	0.9562×10^{-3}	0.6872×10^{-3}
$t = 0$	0.1956×10^{-2}	0.4035×10^{-3}	0.2411×10^{-3}
$t = 1$	0.2838×10^{-3}	0.2428×10^{-3}	0.2552×10^{-3}

optimal initial condition is achieved by minimization of the cost function, while the RMSE is used as a measure of the quality of optimal initial condition. The former mainly concerns the mismatch between the model solution with the observation at the observational sites, while the latter concerns the mismatch of the model solution with the exact one at the model grid points. Figure 10 plots the portion of the mismatch of the model solution with the observation at the observational sites

$$\sum_{s=1}^{2}\sum_{k=1}^{K}\left(\{H[S(t_s)u_0(x_k)]\} - \left(y_s^k\right)^2\right. . \tag{20}$$

It is seen that no such jumps are observed at $M = 61$ and 81. The observation, the optimal initial conditions by linear interpolation and the fifth-order Lagrange interpolation are plotted in Fig. 11 at the observational sites. Using a fifth-order Lagrange interpolation for the operator H, in comparison to linear interpolation, yields a better optimal initial condition.

7. Error control: Illustrative example

The error control methodology in Section 3 is applied to the canonical Burgers problem (9) whose spatially discrete version [the so-called modified equation (Warming and Hyett, 1974)] reads

$$\begin{cases} \dfrac{\mathrm{d}\mathbf{u}}{\mathrm{d}t} = F(x, \mathbf{u}) + E, \\ \quad (x, t) \in (-1, 1) \times (0, \infty), \\ \text{Boundary Condition: } \mathbf{u}(-1, t) = 0, \mathbf{u}(1, t) = 0 \ \forall t \in (0, \infty), \\ \text{Initial Condition: } \mathbf{u}(x, 0) = U. \end{cases} \tag{21}$$

Here $E = \sum_p \varepsilon(p)[\frac{\partial^p u}{\partial x^p}]$ where $\varepsilon(p)$ denotes the coefficient of the pth spatial derivative. As the Burgers equation is discretized by a formally second-order accurate scheme, in order to control the dominant numerical diffusion error, the discretization error E can be expanded as

$$E = \sum_{j=1}^{J_{\max}} \varepsilon_j X_j, \tag{22}$$

where X_j are the eigenvectors of the fourth-order operator $[\frac{\partial^4 u}{\partial x^4}]$. To control the total discretization error, it should be expanded in terms of the appropriate eigenvectors of the error covariance matrix. These eigenvectors can be computed by the Monte Carlo approach: the model is integrated with many samples of initial conditions, which are obtained from the exact one superimposed by Gaussian noise with zero mean and variance $\sigma = 0.075$. Here 9999 samples are used to approximate the covariance matrix; its eigenvectors X_j are obtained using LAPACK; and the parameter vector $\vec{\varepsilon} = (\varepsilon_1, \varepsilon_2, \ldots, \varepsilon_{J_{\max}})$ is determined by the 4D-Var approach with the cost function defined by eq. (8), where $\alpha = 0$.

Figure 12 plots the evolution of the RMSE of the numerical solution of the modified Burgers equation (with reference to the exact one). The results in Fig. 12a correspond to the error term E being represented by the eigenvectors associated with

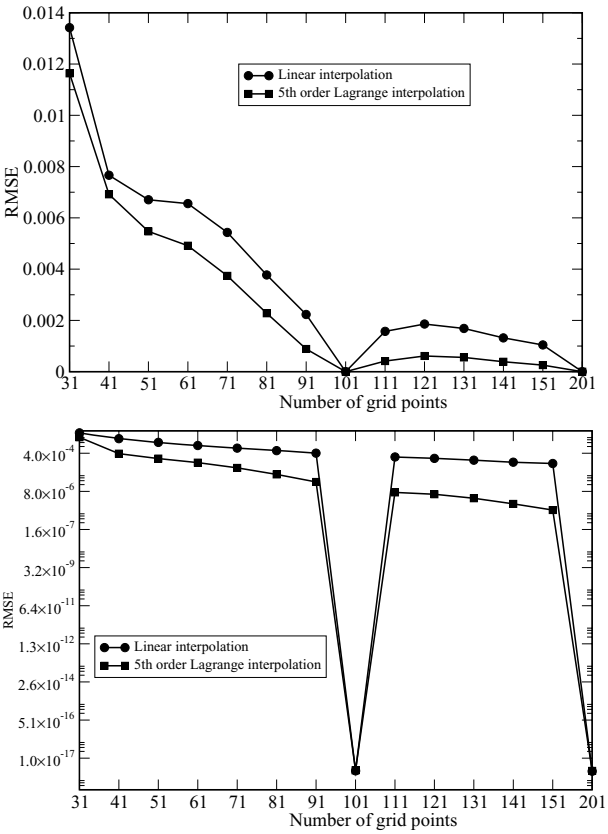

Fig. 8. RMSE of the exact solutions interpolated on to the observation sites at (a) $t = 0$ and (b) $t = 1$.

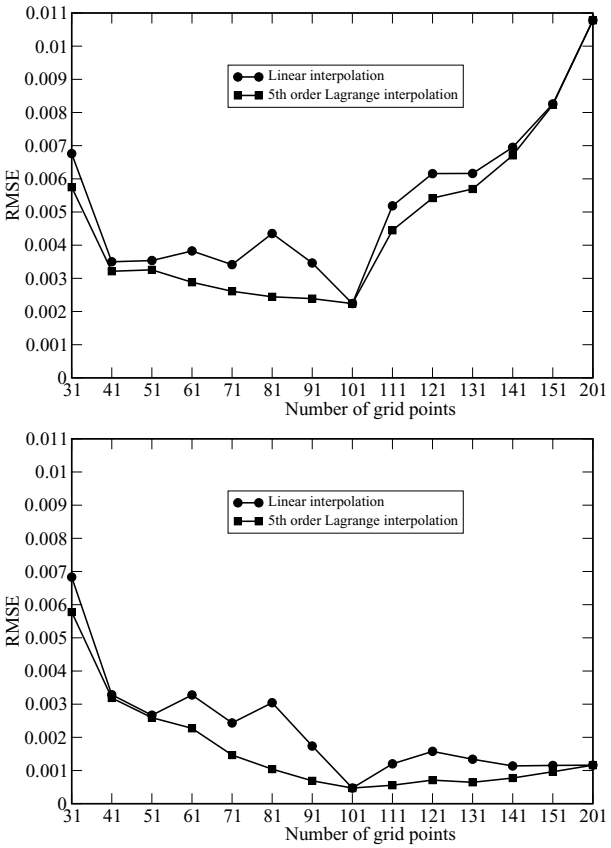

Fig. 9. RMSE of the optimal initial condition relative to the exact one with background perturbation variance (a) $\sigma = 0.025$ and (b) $\sigma = 0.0025$.

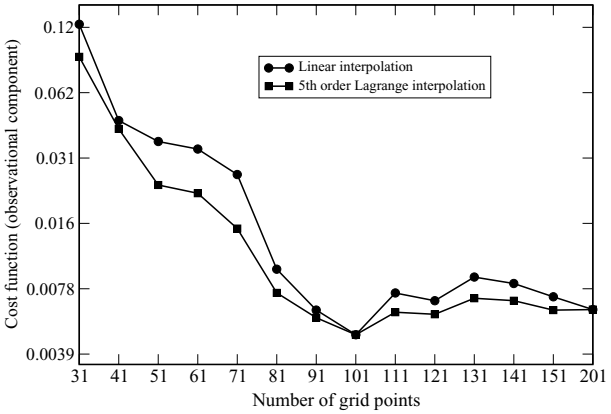

Fig. 10. Observational cost function versus model resolution.

the first 10, 20 and 29 largest eigenvalues, while in Fig. 12b they correspond to the eigenvectors associated with the first 10, 20 and 29 smallest eigenvalues of the fourth-order derivative operator with homogeneous Dirichlet boundary conditions. It is observed that the eigenvectors corresponding to the smallest eigenvalues better represent the discretization error, implying that the discretization error is related to small scales of the flow.

The results are further improved if we approximate E by

$$E = \sum_{i=1}^{N_t} \sum_{j=1}^{J_{\max}} \varepsilon_{ij} \phi_i(t) X_j, \tag{23}$$

where N_t is the number of subintervals of the time domain (0,T), and $\phi_i(t)$ is piecewise constant on the temporal domain (0, 1):

$$\phi_i(t) = \begin{cases} 1 \text{ if } \dfrac{i-1}{N_t} \le t \le \dfrac{i}{N_t}, \; i \text{ temporal subdivision index.} \\ 0 \text{ elsewhere} \end{cases} \tag{24}$$

Figure 13 illustrates the result with $N_t = 5$ and $T = 1$. The RMSEs are greatly reduced throughout the entire assimilation window, especially in the middle.

Finally, it is pointed out that since all of the independent eigenvectors of either the fourth-order derivative operator or the error covariance matrix form a complete basis of the solution space, they should represent the same error term if all of the eigenvectors of either operator are used. There is no need to combine them to correct the error.

8. Summary and conclusions

In summary we make the following remarks.

(i) When the model resolution is coarse relative to observation, both the discretization error and the projection error are relatively large. Although the observation improves the initial condition through the data assimilation process, the optimal initial condition still deviates from the true one, and it is found to be insensitive to the background.

(ii) With an increase in model resolution, the model and projection errors naturally decrease. The optimal initial condition is obtained under the balance between the error statistics of the background and the observation. There exists a local minimum of the RMSE (with reference to the true one) of the optimal initial condition, that is, there is an optimal resolution of the model which permits effective use of observation.

(iii) When the model resolution increases further beyond that of the observation, the optimal initial condition becomes sensitive to the background, that is, the error of the background dominates in the data assimilation process.

(iv) Prediction can be improved by controlling errors represented by additional terms in the model equation. If we have some a priori knowledge of error behaviour (as in the case of discretization error), then the model can be augmented with appropriate correction terms to reduce this error. In the absence of any such knowledge, the error can be represented by the eigenfunctions of the error covariance matrix.

(v) Increasing the resolution of observation does not necessarily translate into improved assimilation. In fact, if the model

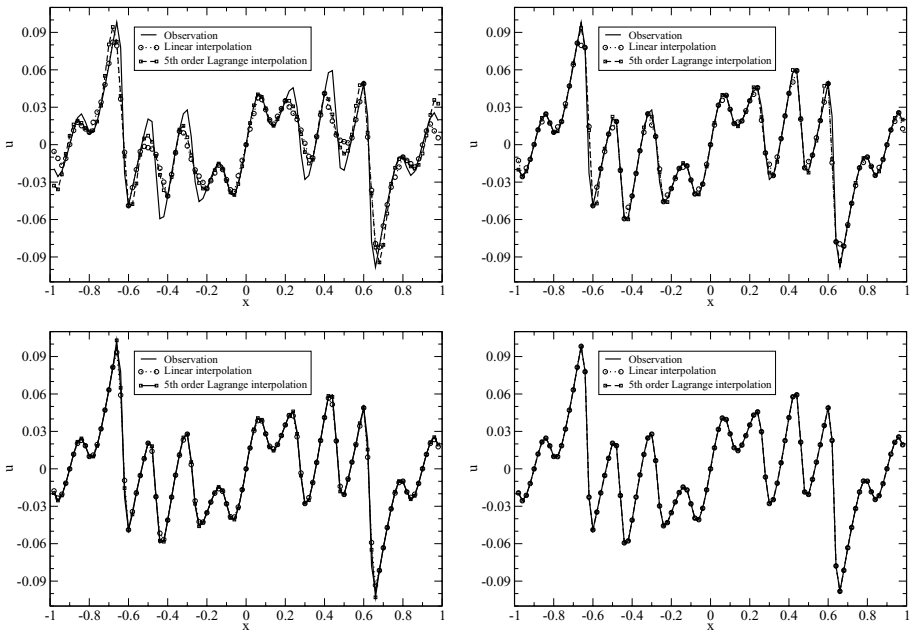

Fig. 11. The observations and the exact solutions interpolated on to the observation sites.

solution is not sufficiently resolved high density of observation degrades the data assimilation process and prediction.

The sensitivity of the optimal initial condition to the background can be explained as follows. When the model resolution is relatively coarse, the minimization problem is 'overdetermined.' The observation itself, if its quality is good enough, can determine the optimal initial condition without knowledge of the background. However, if the model resolution is finer than that of the observation, the minimization problem is 'underdetermined.' The observation alone does not suffice to determine the optimal initial condition and the background assumes some importance.

The canonical equation dealt with in this study is a convection-diffusion equation with a forcing term, which is supposed to model external forces in meteorological/oceanographical applications stemming from the solar radiation, the topography, or the air/sea flux exchange, etc. It precludes baroclinic instability, and as such its applicability to such situations is rather limited. Discretization normally introduces diffusion and dispersion errors into any instability wave analysis thereby dissipating its energy and affecting its phase velocity (e.g. see Zang et al., 1989). Although the model is simple and the observations synthetic and uniformly distributed, the conclusions of this study should hold. These conclusions based on the ideal situation represent the bottom line, and these trends will become more pronounced in a real situation.

Observational error can be included in the present analysis. However, it requires a second-order adjoint formulation, which is the subject of our continuing work.

9. Acknowledgments

This work was initiated under the auspices of the Center for Earth Surface Processes Research (CESPR). Francois Le Dimet acknowledges with pleasure the financial support of CESPR. Pierre Ngnepieba and Yonghui Wu were supported by the Office of the Provost at Florida State University. We thank Nocedal for providing the L-BFGS code. We thank the reviewers for their comments, which helped in enhancing the clarity of presentation.

10. Appendix A: Exact solution of burgers equation

The classical Burgers equation (Burgers, 1948; Platzman, 1964; Benton and Platzman, 1972),

$$\frac{\partial u}{\partial t} + u\frac{\partial u}{\partial x} = \mu\frac{\partial^2 u}{\partial x^2} \quad (x,t) \in (-1,1)\times(0,\infty). \tag{A1}$$

has a solution $u(x,t) = -2\mu\frac{1}{\theta}\frac{\partial\theta}{\partial x}$ (Hopf–Cole transformation) where θ $(x,\ t)$ is a positive (negative) solution of the one-dimensional heat equation,

$$\frac{\partial\theta}{\partial t} = \mu\frac{\partial^2\theta}{\partial x^2}, \quad (x,t) \in (-1,1)\times(0,\infty). \tag{A2}$$

Assume that the solution of the heat equation is of the form

$$\theta(x,t) = C + \sum_{i=1}^{N} C_i \exp\left[-\mu(k_i\pi)^2 t\right]\cos(k_i\pi x), \tag{A3}$$

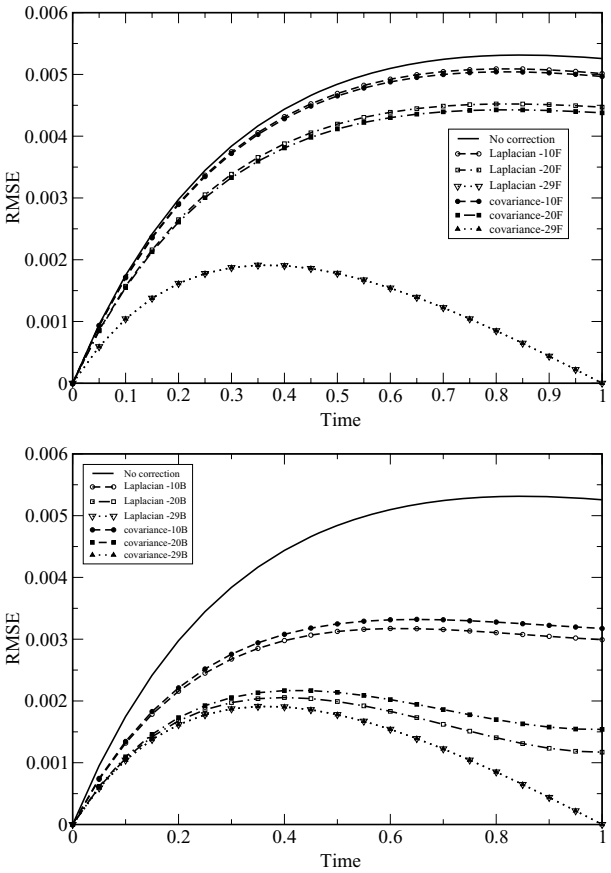

Fig. 12. Comparison of the evolution of RMSE of the solutions for the modified model based on the eigenvectors of the Laplacian operator and the negative error covariance matrix. The model resolution is $M = 31$.

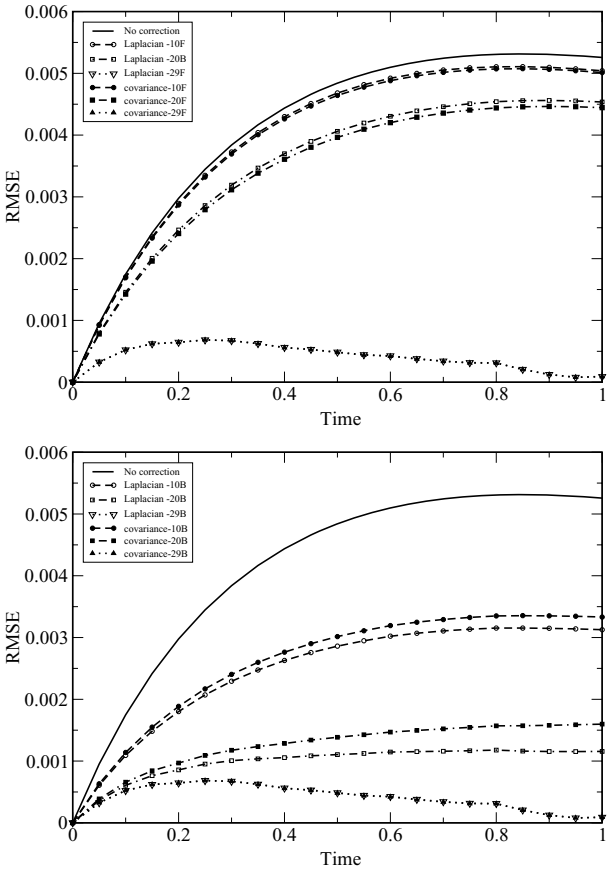

Fig. 13. Same as Fig. 12 with five piecewise-constant subintervals of the time domain (0, 1).

where N and $k_i (i = 1, 2, \ldots, N)$ are positive integers. C and C_i are real number. The solution of (A1) can be written as

$$u(x,t) = -2\mu \frac{1}{\theta}\frac{\partial \theta}{\partial x} = 2\mu\pi \frac{\sum_{i=1}^{N} C_i k_i \exp\left[-\mu(k_i\pi)^2 t\right] \sin(k_i \pi x)}{C + \sum_{i=1}^{N} C_i \exp\left[-\mu(k_i\pi)^2 t\right] \cos(k_i \pi x)}. \quad \text{(A4)}$$

In a real situation, there is always some external force in the weather/climate model, stemming from the solar radiation, the topography, or the air/sea flux exchange, etc. To incorporate external force in our model, we rewrite the Hopf–Cole transformation:

$$u(x,t) = -2\mu \frac{\theta_x}{\theta} + a(x), \quad \text{(A5)}$$

where $a(x)$ is a known function. The corresponding Burgers equation is

$$\frac{\partial u}{\partial t} + u\frac{\partial u}{\partial x} - \mu \frac{\partial^2 u}{\partial x^2} = \frac{\partial [a(x)u]}{\partial x} + f(x), \quad \text{(A6)}$$

where $f(x) = -[a(x)a'(x) + \mu a''(x)]$. Assume $a(x) = \alpha_1 \sin(l_1\pi x) + \alpha_2 \sin(l_2\pi x)$ with k_i positive integers and α_i real numbers for $i = 1, 2$. We have further that

$$\begin{aligned} &\frac{\partial u}{\partial t} + u\frac{\partial u}{\partial x} - \mu\frac{\partial^2 u}{\partial x^2} - \frac{\partial}{\partial x}[\alpha_1 \sin(l_1\pi x)u + \alpha_2 \sin(l_2\pi x)u] \\ &= -\pi[\alpha_1 \sin(l_1\pi x) + \alpha_2 \sin(l_2\pi x)][\alpha_1 k_1 \cos(l_1\pi x) \\ &\quad + \alpha_2 k_2 \cos(l_2\pi x))] + \mu\pi^2\left[\alpha_1 k_1^2 \sin(l_1\pi x) + \alpha_2 k_2^2 \sin(l_2\pi x)\right]. \end{aligned} \quad \text{(A7)}$$

For the well posedness of the problem, homogeneous Dirichlet boundary conditions are imposed.

Let θ be of the form (A3). Then the solution of the forced Burgers eq. (A6) is

$$u(x,t) = \alpha_1 \sin(l_1\pi x) + \alpha_2 \sin(l_2\pi x) + 2\mu\pi \frac{\sum_{i=1}^{N} C_i k_i \exp\left[-\mu(k_i\pi)^2 t\right] \sin(k_i \pi x)}{C + \sum_{i=1}^{N} C_i \exp\left[-\mu(k_i\pi)^2 t\right] \cos(k_i \pi x)}. \quad \text{(A8)}$$

Specifically, we set $N = 3$, $k_1 = 2$, $k_2 = 5$, $k_3 = 11$, $C_1 = 5$, $C_2 = 1$, $C_3 = 2$, $C = 8.1$, $l_1 = 2$, $l_2 = 5$, $\alpha_1 = 0.02$, $\alpha_2 = 0.015$

and $\mu = 0.001$. The solution of (A6) is

$$u_{\rm ex}(x,t) = 0.02\sin(2\pi x) + 0.015\sin(5\pi x) + 0.002\pi \times \frac{n1(t)+n2(t)+n3(t)}{d1(t)+d2(t)+d3(t)}, \tag{A9}$$

where $n1(t)$, $n2(t)$, $n3(t)$, $d1(t)$, $d2(t)$ and $d3(t)$ are defined as follow.

$$\begin{aligned} n1(t) &= 10\exp(-0.004\pi^2 t)\sin(2\pi x)\\ n2(t) &= 5\exp(-0.025\pi^2 t)\sin(5\pi x)\\ n3(t) &= 22\exp(-0.121\pi^2 t)\sin(11\pi x)\\ d1(t) &= 8.1 + 5\exp(-0.004\pi^2 t)\cos(2\pi x)\\ d2(t) &= \exp(-0.025\pi^2 t)\cos(5\pi x)\\ d3(t) &= 2\exp(-0.121\pi^2 t)\cos(11\pi x). \end{aligned} \tag{A10}$$

It is easy to verify that $u(x,t)$ satisfies the zero Dirichlet boundary condition. The exact initial state is

$$U(x) = u_{\rm ex}(x,0) = 0.02\sin(2\pi x) + 0.015\sin(5\pi x) + 0.002\pi\,\frac{10\sin(2\pi x)+5\sin(5\pi x)+22\sin(11\pi x)}{8.1+5\cos(2\pi x)+\cos(5\pi x)+2\cos(11\pi x).} \tag{A11}$$

References

Benton, E. and Platzman, G. 1972. A table of solutions of the one-dimensional Burgers Equation. *Quart. Appl. Math.* July, 195–212.

Burgers, J. M. 1948. Mathematical model illustrating the theory of turbulence. *Adv. Appl. Mech.* **1**, 171–199.

Dalcher, A. and Kalnay, E. 1987. Error growth and predictability in operational ECMWF forecasts. *Tellus* **39A**, 474–491.

Derber, J. C. 1989. A variational continuous assimilation technique. *Mon. Wea. Rev.* **117**, 2427–2446.

Gilbert, J. C. and Lemaréchal, C. 1989. Some numerical experiments with variable storage quasi-Newton algorithms. *Math. Prog.* **45**, 407–435.

Griffith, A. K. and Nichols, N. K. 2000. Adjoint methods in data assimilation for estimating model error. *Tellus* **55A**, 1–15.

Le Dimet, F.-X. and Talagrand, O. 1986. Variational algorithms for analysis and assimilation of meteorological observations: theoretical aspect. *Tellus* **38A**, 97–110.

Leredde, Y., Lellouche, J. M., Devenon, J. L. and Dekeyser, I. 1998. On initial boundary conditions and viscosity coefficient control for Burgers' equation. *Int. J. Numer. Methods Fluids* **28**, 113–128.

Liu, D. C. and Nocedal, J. 1989. On the limited memory BFGS method for large scale optimization. *Math. Prog.* **45**, 503–528.

Nicolis, C. 2003. Dynamics of model error: some generic features. *J. Atmos. Sci.* **60**, 2208–2218.

Paun, I., Blum, J. and Charpentier, I. 2003. Utilisation des bases d'ondelettes pour la reduction du coût de l'assimilation de données dans un modèle de circulation oceanique. Annals of University of Craiova, *Math. Comp. Sci. Ser.* **30**, 188–197.

Platzman, G. 1964. An exact integral of complete spectral equations for unsteady one-dimensional flow. *Tellus* **16**, 422–431.

Richtmyer, R. and Morton, K. 1967. *Difference Methods for Initial-Value Problems*. Interscience Publishers, New York, USA .

Tribbia, J. J. and Baumhefner, D. P. 1988. The reliability of improvements in deterministic short-range forecasts in the presence of initial state and model deficiencies. *Mon. Wea. Rev.* **116**, 2276–2288.

Uboldi, F. and Kamachi, M. 2000. Time-space weak-constraint data assimilation for nonlinear models. *Tellus* **52A**, 412–421.

Warming, R. F. and Hyett, B. J. 1974. The modified equation approach to the stability and accuracy analysis of finite-difference. *J. Comput. Phys.* **14**, 197–179.

Zang, T. A., Krist, E. K. and Hussaini, M. Y. 1989. Resolution requirements for numerical simulations of transition. *J. Scient. Comput.* **4**(2), 159–217.